Spherical Image-Based Visual Servo and Structure Estimation

Peter I. Corke

Abstract— This paper presents a formulation of image-based visual servoing (IBVS) for a spherical camera where coordinates are parameterized in terms of colatitude and longitude: IBVS-Sph. The image Jacobian is derived and simulation results are presented for canonical rotational, translational as well as general motion. Problems with large rotations that affect the planar perspective form of IBVS are not present on the sphere, whereas the desirable robustness properties of IBVS are shown to be retained. We also describe a structure from motion (SfM) system based on camera-centric spherical coordinates and show how a recursive estimator can be used to recover structure. The spherical formulations for IBVS and SfM are particularly suitable for platforms, such as aerial and underwater robots, that move in $SE(3)$.

I. INTRODUCTION

Visual servoing is the use of information from one or more cameras to guide a robot to achieve a task [1], [2]. Image-Based visual servoing (IBVS) is a robust and efficient technique where the task is defined in terms of the desired view of the target and a control law is synthesized to move the camera toward that view. The goal pose is defined *implicitly* in the desired view. The pose of the target does not need to be known apriori, the robot moves toward the observed target wherever it might be in the workspace. Image-based control can be considered as an inverse problem to optical flow — given a current and desired view the required optical flow can be computed. The problem is to synthesize a controller to command the required motion in SE(3) to achieve the desired flow.

The controllers typically used are based on a linearization of the system kinematics, the image Jacobian, and are technically only a local method. However in practice IBVS demonstrates a remarkably large field of convergence and robustness to errors in camera calibration and the range of target points. One well known problem occurs for the case of large rotation about the optical axis of the camera where the camera moves away from the target as it rotates and then back again — a phenomenon known as *camera retreat* [3]. This behaviour leads to inefficient trajectories which can cause robot joint limits to be exceeded. In [3] the camera retreat effect is explained intuitively by the fact that the IBVS control law causes feature points to move in straight lines on the image plane. However for a rotating camera the points move along circular arcs. The linear controller resolves this by changing the overall scale dynamically in order that motion along arcs appears as straight line motion. The scale change is achieved by z-axis translation.

School of Engineering Systems, Queensland University of Technology, Brisbane, Australia. `peter.corke@qut.edu.au`
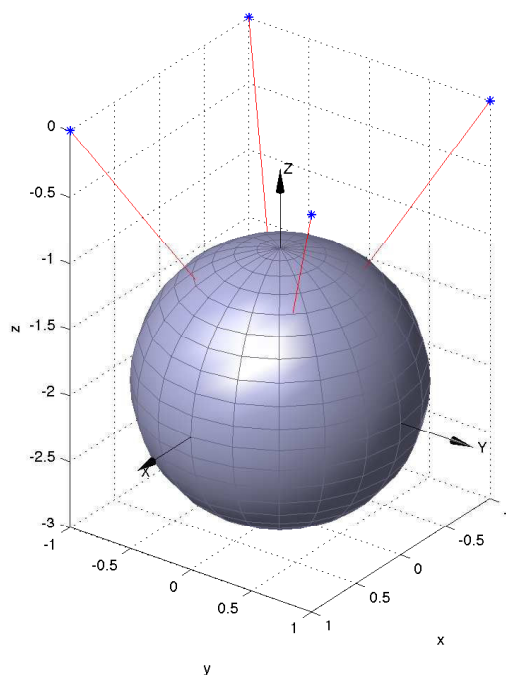

Fig. 1.   IBVS on the sphere. Showing the goal pose for simulation and the four point features.

This intuition about the failure mode [3] leads us to consider the use of different coordinate systems. Polar [4], [5], or cylindrical [6], coordinate systems have been proposed where a point feature is represented by a distance, r, and angle θ with respect to the center of fhe image instead of its Cartesian coordinates. For large optical-axis rotation the required feature motion is now a straight line parallel to the θ axis. Similarly a pure scale change (z-axis translation) would cause radial motion of the points which corresponds to motion parallel to the r axis.

The polar coordinate formulation (IBVS-P), like the classical Cartesian one, is based on visual features sensed using a "standard" perspective camera. In the last few years there has been growing interest in spherical imaging, where the image "plane" (more correctly surface) is considered to be a unit sphere [7], [8], see Figure 1. A wide perceptual field is important for many robotic competencies such as path planning and collision avoidance and this has led researchers to adopt, or develop, wide-angle viewing systems [9]–[11]. For example, a typical perspective cameras with a field of view angle of $60\,\mathrm{deg}$ has a solid angle of approximately $1\,\mathrm{sr}$ which is less than 1/6th of a hemisphere. The perspective transform has a singularity for rays at $90\,\mathrm{deg}$ from the optical

axis, and lenses capable of wide field-of-view are either expensive or have significant distortion near the periphery of the image. Fisheye and catadioptric camera systems have been used [11], [12] for robotic wide-angle imaging and can have fields of view well above $2\pi\,\mathrm{sr}$ but result in highly distorted images (but which can be well modeled).

For these reasons we consider visual servoing for wide-angle non-perspective imaging and in particular visual servoing on the sphere: IBVS-Sph. Spherical imaging has other advantages for visual servoing. Firstly, a spherical camera eliminates the need to explicitly keep features in the field of view which is a problem with both position-based visual servoing and some hybrid schemes. Secondly, for a perspective camera there is ambiguity between R_x and $-T_y$ motion (and R_y and $-T_x$ motion) which can lead to slow convergence and/or sensitivity to noise in feature coordinates.

There has been relatively little work on spherical visual servoing. Fomena and Chaumette [13] consider the case for a single spherical target from which they extract features derived from the projection to the spherical imaging plane, a circle, the center of the circle, and the apparant radius. Tahri et al. [14] consider spherical image features such as lines and moments. Hamel and Mahony [7] describe kino-dynamic control of an underactuated aerial robot using point features. They observe that only the image geometry of a spherical camera preserves the passivity-like properties of the body fixed frame dynamics of a rigid object in the image space. In all these works a unit vector, a redundant parameterization, is used to represent points on the sphere.

In this paper we consider IBVS on an ideal spherical image "plane" with point features projected onto a sphere and represented by their angles of colatitude and longitude. The unified imaging model [15] provides a means to transform images, or features, from different types of cameras, perspective, fisheye or catadioptric on to the sphere where they can be treated uniformly. This has advantages over trying to formulate IBVS controllers for the many different projection models that are possible for wide angle cameras such as equiangular, stereographic, equisolid etc. It also has the advantage that conventional robotic sensors can also be projected onto the image plane, for example the gravity vector, magnetic field vector or angular velocity [16].

The contributions of this paper are the derivation of the Jacobian for IBVS on the sphere using an angular parameterization of colatitude and longitude, and investigation of the performance of the resulting controller. The paper also develops a camera-centric structure-from-motion technique where the depth map is defined on the surface of the sphere.

The next section, Section II, derives the optical flow equation and image Jacobian for the sphere, and then in Section III the IBV-Sph control scheme is outlined. Section IV presents simulation results for canonical motions along and about the different axes as well as for general motion. Section V recalls the unified imaging model that can be used to create a spherical image from one or more cameras that could be perspective, fisheye or catadioptric. Section VI outlines camera-centric structure-from-motion technique and
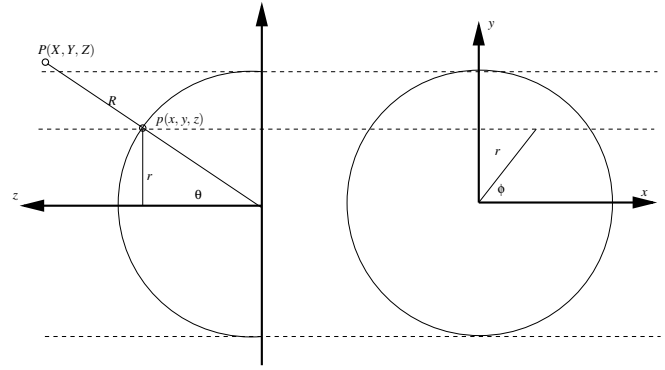

Fig. 2. The coordinate system. P is a world point, mapped to p on the surface of the unit sphere represented by the angles θ and ϕ.

presents further simulation results.

II. IMAGE JACOBIAN FOR SPHERICAL IBVS

We follow a similar approach to that used for the perspective camera [1] and assume that the camera is moving with translational velocity $\mathbf{T} = (t_x,\,t_y,\,t_z)$ and angular velocity $\omega = (\omega_x,\,\omega_y,\,\omega_z)$ in the camera frame. A world point, $\mathbf{P}$, with camera-relative coordinates $^c\mathbf{P} = (X,\,Y,\,Z)^T$ has camera-relative velocity

$$^c\dot{\mathbf{P}} = -\,^c\omega_e \times\,^c\mathbf{P} + \,^c\mathbf{T}_e \tag{1}$$

which can be written in scalar form as

$$\dot{x} = z\omega_y - y\omega_z + t_x \tag{2}$$
$$\dot{y} = x\omega_z - z\omega_x + t_y \tag{3}$$
$$\dot{z} = y\omega_x - x\omega_y + t_z \tag{4}$$

The world point P is projected, Figure 2, to point p on the surface of a unit sphere centered at the origin

$$x = \frac{X}{R},\ \ y = \frac{Y}{R},\ \text{and}\ \ z = \frac{Z}{R} \tag{5}$$

where the focal point is at the center of the sphere and the radial distance to the point is $R = \sqrt{X^2 + Y^2 + Z^2}$. The spherical surface constraint $x^2 + y^2 + z^2 = 1$ means that one of the Cartesian coordinates is redundant, and we will instead use a minimal spherical coordinate system comprising the angle of colatitude

$$\theta = \sin^{-1} r,\ \theta = [0,\,\pi) \tag{6}$$

and the azimuth angle

$$\phi = \tan^{-1}\frac{y}{x},\ \phi = [-\pi,\,\pi) \tag{7}$$

yielding the point feature vector $\mathbf{f} = (\theta,\,\phi)$. Note that any minimal representation admit singularities, in this case at the poles. Note also that motion on this plane is in general not a great circle on the sphere — only motion along lines of colatitude and the equator are great circles.

Taking the derivatives of (6) and (7) with respect to time and substituting (2) – (4) as well as

$$X = R\sin\theta\cos\phi,\ Y = R\sin\theta\sin\phi,\ Z = R\cos\theta \tag{8}$$

5551

Target points	$(\pm 1, \pm 1, 0)$
Goal position	$(0, 0, -2)$
Gain γ	0.001
θ^*	0.6155 rad
ϕ^*	$-3\pi/4, -\pi/4, \pi/4, 3\pi/4$

TABLE I

SIMULATION PARAMETERS.

we obtain, in matrix form, the spherical optical flow equation

$$\left[\begin{array}{c} \dot{\theta} \\ \dot{\phi} \end{array} \right] = \mathbf{J}(\theta, \phi, R) \left[\begin{array}{cccccc} t_x & t_y & t_z & \omega_x & \omega_y & \omega_z \end{array} \right]^T \quad (9)$$

where (10) — next page — is the image feature Jacobian or optical flow equation in terms of the *spherical* point feature $\mathbf{f} = (\theta, \phi)$. A spherical Jacobian, with respect to translation only, was described in [17].

There are important similarities to the Jacobian derived for the projective camera in polar coordinates [5], [6]. Firstly, the constant elements 0 and 1 fall at the same place, indicating that colatitude is invariant to rotation about the optical axis, that azimuth angle is invariant to optical axis translation, but equal to optical axis rotation. As for all image Jacobians the translational sub-matrix (the first 3 columns) is a function of point depth $1/R$. Note also that the second row of the Jacobian is not defined at the poles where $\sin \theta = 0$ and azimuth has no meaning.

We can also partition the Jacobian [3] into a translational and rotational part

$$\left[\begin{array}{c} \dot{\theta} \\ \dot{\phi} \end{array} \right] = \frac{1}{R}\mathbf{J}_t(\theta, \phi) \left[\begin{array}{c} t_x \\ t_y \\ t_z \end{array} \right] + \mathbf{J}_\omega(\theta, \phi) \left[\begin{array}{c} \omega_x \\ \omega_y \\ \omega_z \end{array} \right] \quad (11)$$

which is important for both control and structure estimation. For points at infinity the first term will be zero yielding a simple relationship between optical flow and angular velocity. For a mobile robot moving in $SE(3)$ the vector $(\omega_x, \omega_y, \omega_z)$ can be measured using a gyroscope which leads to a simple relationship between optical flow and translational velocity.

III. SPHERICAL IBVS CONTROL LAW

For control purposes we follow the normal procedure of computing one 2×6 Jacobian, (10), for each of N feature points and stacking them to form a $2N \times 6$ matrix

$$\left[\begin{array}{c} \dot{\theta}_1 \\ \dot{\phi}_1 \\ \vdots \\ \dot{\theta}_N \\ \dot{\phi}_N \end{array} \right] = \left[\begin{array}{c} \mathbf{J}_1 \\ \vdots \\ \mathbf{J}_N \end{array} \right] \mathbf{v} \quad (12)$$

The control law is

$$\mathbf{v} = \mathbf{J}^+ \dot{f}^* \quad (13)$$

where $v = \left[\begin{array}{cccccc} t_x & t_y & t_z & \omega_x & \omega_y & \omega_z \end{array} \right]$ is the camera velocity screw and $\dot{f}^*$ is the desired velocity of the features. Typically we choose this to be proportional to feature error

$$\dot{f}^* = -\gamma(f \ominus f^*) \quad (14)$$

where γ is a positive gain, f is the current value of the feature vector, and f^* is the desired value, which leads to locally linear motion of features within the feature space. $\ominus$ denotes modulo subtraction giving the smallest angular distance given that $\theta = [0, \pi)$ and $\phi = [-\pi, \pi)$.

For the case of a point close to the pole singularity we add only the first row of its Jacobian and would need sufficient points to ensure that $\mathbf{J}$ has full rank. Alternatively it would be possible to perform a change of coordinates of the poles.

If the attitude was servoed by a non-visual sensor such as gyroscope, accelerometer or magnetometer then we could use a partitioned IBVS scheme [3] where we would write (11) as

$$\frac{1}{R}\mathbf{J}_t(\theta, \phi) \left[\begin{array}{c} t_x \\ t_y \\ t_z \end{array} \right] = \left[\begin{array}{c} \dot{\theta} \\ \dot{\phi} \end{array} \right] - \mathbf{J}_\omega(\theta, \phi) \left[\begin{array}{c} \omega_x \\ \omega_y \\ \omega_z \end{array} \right] \quad (15)$$

and solve for translational velocity only.

IV. RESULTS

We present simulation results for the cases: pure z-axis rotation, pure x-axis rotation, pure z-axis translation, pure x-axis translation, and general motion about all axes. The cases of pure-y axis rotation and y-axis translation are not presented but are symmetric to the x-axis cases. The simulation parameters are summarized in Table I. We assume, for now, that the range of each feature point is known exactly.
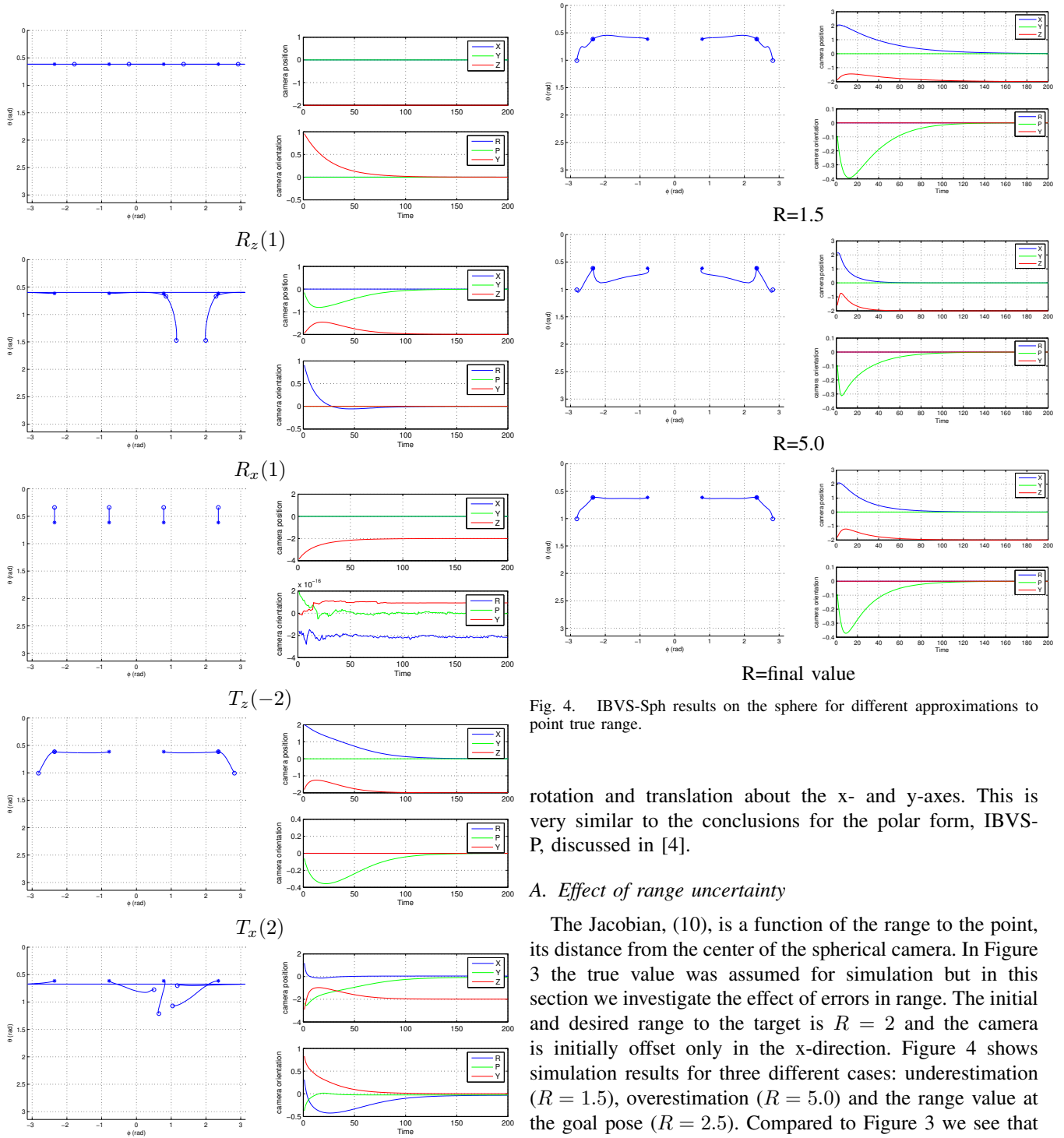
For each simulation we present the feature paths in the $\theta - \phi$ feature space, and the time history of the camera pose shown in terms of translation and rotation in roll-pitch-yaw format. The results are shown in Figure 3 and summarized as:

Rz   has resulted in pure rotation of the camera with no unwanted motion. The features have moved along lines of constant colatitude.

Rx   has resulted in unwanted translational motion in the y-axis and z-axis directions. Two features have had to move more than the others in the colatitude direction.

Tz   has resulted in the desired motion with no unwanted motion. The noise on the attitude is at the limits of arithmetic precision and can be considered as zero. The features have moved along lines of constant longitude.

Tx   has resulted in unwanted translational motion along the z-axis and pitching about the y-axis.

Gen.   the roll angle (rotation about x-axis) has undershot and translation along the y-axis has converged quite slowly.

For the R_x, T_x and general cases the paths on the θ-ϕ plane have been curved rather than straight line motion. This is a consequence of the system's non-linearity. The unwanted motion, observed for the R_x, T_x cases, is a result of cross-coupling terms in (10).

Overall we can conclude that IBVS-Sph handles the cases of pure z-axis rotation and translation very cleanly. While still very satisfactory, it exhibits imperfect decoupling

5552

$$\mathbf{J}(\theta, \phi, R) = \begin{bmatrix} \frac{\cos(\phi)\cos(\theta)}{R(t)} & \frac{\sin(\phi)\cos(\theta)}{R(t)} & -\frac{\sin(\theta)}{R(t)} & \vdots & -\sin(\phi) & \cos(\phi) & 0 \\ -\frac{\sin(\phi)}{R(t)\sin(\theta)} & \frac{\cos(\phi)}{R(t)\sin(\theta)} & 0 & \vdots & -\frac{\cos(\phi)\cos(\theta)}{\sin(\theta)} & -\frac{\sin(\phi)\cos(\theta)}{\sin(\theta)} & 1 \end{bmatrix} \quad (10)$$

$R_z(1)$

$R_x(1)$

$T_z(-2)$

$T_x(2)$

General motion: $T(2, -2, -3)R_x(0.5)R_y(-0.5)R_z(1)$

Fig. 3. IBVS-Sph for various initial poses. (left), the θ-ϕ feature plane where the initial coordinate is marked with a 'o' and the final coordinate marked with a '*'. (right), the evolution of camera Cartesian translation and rotation (RPY format) versus time. Units are in radians and metres.

R=1.5

R=5.0

R=final value

Fig. 4. IBVS-Sph results on the sphere for different approximations to point true range.

rotation and translation about the x- and y-axes. This is very similar to the conclusions for the polar form, IBVS-P, discussed in [4].

A. Effect of range uncertainty

The Jacobian, (10), is a function of the range to the point, its distance from the center of the spherical camera. In Figure 3 the true value was assumed for simulation but in this section we investigate the effect of errors in range. The initial and desired range to the target is $R = 2$ and the camera is initially offset only in the x-direction. Figure 4 shows simulation results for three different cases: underestimation ($R = 1.5$), overestimation ($R = 5.0$) and the range value at the goal pose ($R = 2.5$). Compared to Figure 3 we see that the convergence is slower for the $R = 1.5$ case and faster for the R=5 case which is expected since closed-loop gain for translational DOF is proportional to R. The unwanted z-axis translation is slightly worse for the $R = 5$ case. In all three cases the pitch angle undergoes unwanted motion with a long settling time which is independent of R. In general

5553

though we can conclude that for a significant range of error in point depth the closed-loop response is quite satisfactory. In this respect IBVS-Sph is similar to its perspective-imaging counterpart IBVS.

V. SPHERICAL CAMERAS

True spherical cameras are under development [18], [19] but until they become a reality we must be content with partial spherical views from a camera, or a mosaic view from multiple cameras (such as the Point Grey Ladybug camera).

The unified model of Geyer and Daniilidis [15] provides a convenient framework to consider very different types of cameras such as standard perspective, catadioptric and many types of fisheye lens. The projection model is a two-step process. Firstly, the world point P is projected to the surface of the unit sphere with a focal point at the center of the sphere. The center of the sphere is the origin and the image plane is normal to the z-axis at a distance $-m$. Secondly the point p is re-projected to the image plane using a focal at a distance l along the z-axis, where l is a function of the imaging geometry.

Commonly used mirrors have a parabolic or hyperbolic cross-section, and for these $l = \epsilon$ the eccentricity of the conic section: $l = 1$ for a parabola and $0 < \epsilon < 1$ for a hyperbola. Mirrors commonly used in robotics, for example [9], [20], have an equiangular model and the focal point is not constant for all points in the scene. Theoretically the unified model does not apply to this case (non-central projection) but in practice this difference in focal point is very small compared to the world scale and such mirrors are well approximated by the unified model. Many fisheye cameras can also be included in this framework [21], generally with $l > 1$.

Using the second step of the unified model we can project images captured with wide-angle cameras to the sphere. All common image processing operations can be formulated on the sphere, including spherical SIFT features [22]. Alternatively features could be detected in perspective camera images and projected to the spherical feature plane.

VI. STRUCTURE AND MOTION ESTIMATION ON THE SPHERE

In the IBVS example of the previous section the values of R required to compute the image Jacobian were taken from the simulation engine or approximated. However it is straightforward to estimate point depth by rewriting (11) in identification form as

$$\left(\mathbf{J}_t(\theta, \phi) \begin{bmatrix} t_x \\ t_y \\ t_z \end{bmatrix} \right) (1/R) = \begin{bmatrix} \dot{\theta} \\ \dot{\phi} \end{bmatrix} - \mathbf{J}_\omega(\theta, \phi) \begin{bmatrix} \omega_x \\ \omega_y \\ \omega_z \end{bmatrix} \tag{16}$$

or

$$\mathbf{A}\Theta = \mathbf{b} \tag{17}$$

where and $(\dot{\theta}, \dot{\phi})$ is the optical flow which is observed during the motion and the camera motion $(t_x, t_y, t_z, \omega_x, \omega_y, \omega_z)$ is known, since IBVS commands it. Camera velocity could also be measured — the rotational component quite easily

using a gyroscope, the translational component with more difficulty in practice.

This a spherical form of the classical structure from motion (SfM) problem [23]. Here we consider the scene in camera-centric form as a spherical depth map $D : \mathbb{S}^2 \to \mathbb{R}$. For discrete features we maintain a list of (θ, ϕ, R) tuples. This form makes it trivially easy to handle camera rotational motion, the depth map "rolls around the sphere". For translational camera motion the feature points move over the sphere according to the direction of translation and the point's range. This form of depth map concisely represents the local environment and camera centric depth is used to predict optical flow for the estimator and also to assist the tracker in following features from one frame to the next, reducing computational cost compared to a Cartesian map representation. Uncertainty can also be represented in just 1 DOF per feature.

In the simulation we consider 20 random feature points uniformly distributed within a $10 \times 10 \times 10$ volume. The camera moves from corner to the other and estimates the range of points at each time step. As with all SfM and SLAM techniques we assume that point correspondence is known precisely. World points that are inside the unit sphere during the motion are not updated for that time step.

The range to feature points from the camera center during motion is shown in Figure 5 and varies continuously as the camera moves. Many estimation techniques can be brought to bear on this problem to account for noise in the estimates of optical flow, camera velocity and spherical angles of the feature itself. For example an EKF is often used in structure from motion systems. Alternatively a particle filter could be used and would better model the non-Gaussian distribution of depth uncertainty. In this simulation we used a simple $\alpha - \beta$ tracking filter driven by the scalar solution to (17).

At any time during the motion we can reproject the camera-centric world model to Cartesian coordinates as shown in Figure 6. The median error between estimated and actual feature points is 0.1561 or 1.5% of the size of the dimension of the simulation volume.

VII. CONCLUSIONS

In this paper we have presented a formulation of image-based visual servoing for a spherical camera: IBVS-Sph. Points are projected onto the surface of a unit sphere and described by two angles: colatitude and azimuth. This parameterization is minimal but contains a singularity at the poles for one row of the Jacobian, which in practice is not a significant issue if enough other points are available for control. In the future it would be interesting to study other surfaces, perhaps a torus, or other parameterizations of points on a sphere such as the Mercator projection.

The image Jacobian was derived and simulation results were presented for rotational, translational and general motion. Problems with large rotations that affect the planar perspective form of IBVS are not present on the sphere, whereas the desirable robustness properties of IBVS such as uncertainty of point depth were shown to have been retained.
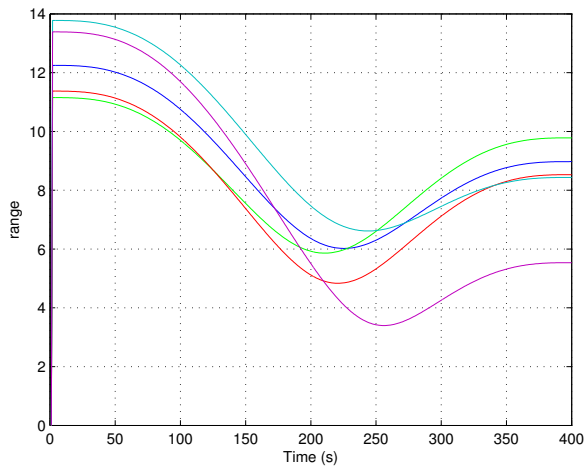
Fig. 5. The range of a subset of points with respect to the camera over its trajectory.
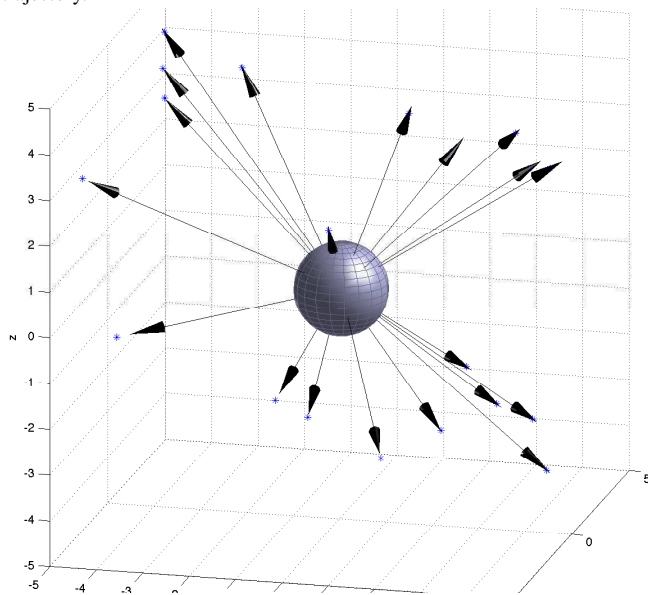

Fig. 6. A snapshot of the spherical depth map part way through the motion. The arrows represent the features estimates in (θ, ϕ, R) form, and the '*' are the true location of the features.

Simulation results show well behaved control responses even for large rotations, although with some cross coupling evident for translational and rotational motion involving the x- and y-directions.

The unified imaging model of Geyer and Daniilidis can be used to map many different types of cameras to the sphere where IBVS-Sph can then be applied. The less attractive alternative is to formulate the Jacobian for every different type of camera projection.

We also described a spherical structure from motion (SfM) system based on camera-centric spherical coordinates and show how a simple estimator can be used to recover scene structure. Future work includes a spherical SLAM system which is similar to the bearing-only SLAM problem. The spherical formulations for IBVS and SfM are particularly suitable for robots that move in $SE(3)$ such as aerial and underwater robots.

REFERENCES

[1] S. Hutchinson, G. Hager, and P. Corke, "A tutorial on visual servo control," *IEEE Transactions on Robotics and Automation*, vol. 12, pp. 651–670, Oct. 1996.

[2] F. Chaumette and S. Hutchinson, "Visual servo control. i. basic approaches," *Robotics & Automation Magazine, IEEE*, vol. 13, pp. 82–90, Dec. 2006.

[3] P. Corke and S. A. Hutchinson, "A new partitioned approach to image-based visual servo control," *IEEE Trans. Robot. Autom.*, vol. 17, pp. 507–515, Aug. 2001.

[4] P. I. Corke, F. Spindler, and F. Chaumette, "Combining Cartesian and polar coordinates in IBVS," in *Proc. Int. Conf on Intelligent Robots and Systems (IROS)*, pp. 5962–5967, 2009.

[5] F. Chaumette and S. Hutchinson, "Visual servo control. ii. advanced approaches [tutorial]," *Robotics & Automation Magazine, IEEE*, vol. 14, pp. 109–118, March 2007.

[6] M. Iwatsuki and N. Okiyama, "A new formulation of visual servoing based on cylindrical coordinate system with shiftable origin," in *Intelligent Robots and System, 2002. IEEE/RSJ International Conference on*, vol. 1, pp. 354–359 vol.1, 2002.

[7] T. Hamel and R. Mahony, "Visual servoing of an under-actuated dynamic rigid-body system: An image based approach.," *IEEE Transactions on Robotics and Automation*, vol. 18, pp. 187–198, April 2002.

[8] J. Lim and N. Barnes, "Directions of egomotion from antipodal points," in *CVPR*, IEEE Computer Society, 2008.

[9] D. Strelow, J. Mishler, D. Koes, and S. Singh, "Precise omnidirectional camera calibration," *Computer Vision and Pattern Recognition, IEEE Computer Society Conference on*, vol. 1, p. 689, 2001.

[10] S. K. Nayar, "Catadioptric omnidirectional camera," *Computer Vision and Pattern Recognition, IEEE Computer Society Conference on*, vol. 0, p. 482, 1997.

[11] J. S. Chahl and M. V. Srinivasan, "Reflective surfaces for panoramic imaging," *Applied Optics*, no. 36, pp. 8275–8285, 1997.

[12] F. Schill, R. Mahony, P. Corke, and L. Cole, "Virtual force feedback teleoperation of the insectbot using optical flow," in *Proc. Australian Conf. Robotics and Automation* (J. Kim and R. Mahony, eds.), 2008.

[13] R. T. Fomena and F. Chaumette, "Visual servoing from spheres using a spherical projection model," in *Proc. Int. Conf. Robotics and Automation*, pp. 2080–2085, 2007.

[14] O. Tahri, Y. Mezouar, F. Chaumette, and P. Corke, "Generic decoupled image-based visual servoing for cameras obeying the unified projection model," in *Robotics and Automation, 2009. ICRA '09. IEEE International Conference on*, pp. 1116–1121, May 2009.

[15] C. Geyer and K. Daniilidis, "A unifying theory for central panoramic systems and practical implications," in *Proceedings European Conference on Computer Vision*, June 2000.

[16] P. I. Corke and R. Mahony, "Sensing and control on the sphere," in *Proc. Int. Symp. Robotics Research*, (Luzern), September 2009, to appear in Springer STAR series.

[17] D. Burschka, J. Geiman, and G. Hager, "Optimal landmark configuration for vision-based control of mobile robots," in *IEEE International Conference on Robotics and Automation*, vol. 3, pp. 3917–3922, 2003.

[18] W. Maddern and G. Wyeth, "Development of a Hemispherical Compound Eye for Egomotion Estimation," in *Australasian Conference on Robotics & Automation*, Australian Robotics & Automation Association, 2008.

[19] G. Krishnan and S. K. Nayar, "Towards a true spherical camera," in *Society of Photo-Optical Instrumentation Engineers (SPIE) Conference Series*, vol. 7240 of *Society of Photo-Optical Instrumentation Engineers (SPIE) Conference Series*, Feb. 2009.

[20] P. Corke, D. Strelow, and S. Singh, "Omnidirectional visual odometry for a planetary rover," in *Proceedings International Conference on Intelligent Robots and Systems*, pp. 4007–4012, September 2004.

[21] X. Ying and Z. Hu, "Can we consider central catiodioptric cameras and fisheye cameras within a unified imaging model," in *8th European Conference on Computer Vision*, pp. 442–455, May 2004.

[22] P. Hansen, W. Boles, and P. Corke, "Spherical diffusion for scale-invariant keypoint detection in wide-angle images," in *DICTA '08: Proceedings of the 2008 Digital Image Computing: Techniques and Applications*, pp. 525–532, December 2008.

[23] T. Huang and A. Netravali, "Motion and structure from feature correspondences: a review," *Proceedings of the IEEE*, vol. 82, pp. 252–268, Feb 1994.